# Journal of Materials Chemistry A

Accepted Manuscript


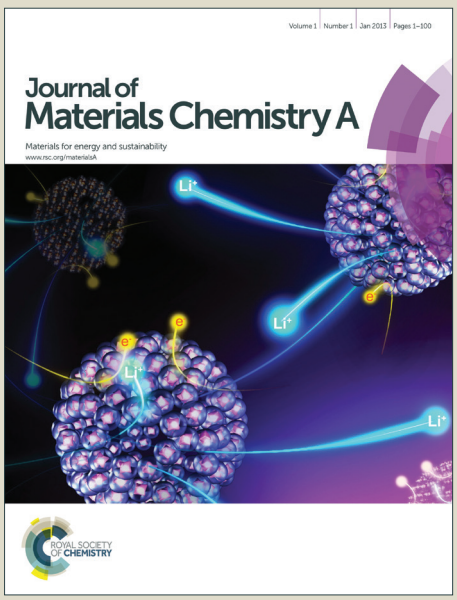





ROYAL SOCIETY OF CHEMISTRY

www.rsc.org/materialsA

Journal Name

ARTICLE

# An Electrochromic Supercapacitor and Its Hybrid Derivatives: Quantifiably Determining Their Electrical Energy Storage by an Optical Measurement

Received 00th January 20xx,
Accepted 00th January 20xx

DOI: 10.1039/x0xx00000x

www.rsc.org/

*Minshen Zhu*[a], *Yang Huang*[a], *Yan Huang*[a], *Wenjun Meng*[a], *Qingchao Gong*[b], *Guangming Li*[b] *and Chunyi Zhi**[a,c]

In this article, an electrochromic supercapacitor was developed with the electrode material active for both electrochromism and energy storage. Detailed measurements of optical spectra of the device revealed that normalized optical density, a concept in electrochromic studies, linearly depended on electrical energy storage (EES) of the supercapacitor. This enabled a precisely quantifiable determination of a solid-state supercapacitor's EES by a simple optical transmission measurement, which is firstly demonstrated to the best of our knowledge. One step further, parallel structured hybrid supercapacitors were designed to integrate the developed smart function with high-performance supercapacitors using polypyrrole (PPy) and manganese oxide ($MnO_2$) as electrode materials. The developed hybrid supercapacitors exhibited excellent capacitive performances and well-maintained ability of electrochromic EES indicator. Different calibration curves can be produced for different types of hybrid supercapacitors. With these curves, EES of hybrid supercapacitors can be precisely determined by a simple optical transmission measurement. Our study paves a way to integrate electrochromic EES indicator to various energy storage devices, as well as promptly and quantitatively determine the EES of various types of supercapacitors by a simple optical transmission measurement.

## 1. Introduction

Developing efficient energy storage devices has attracted a lot of attention because the urgent requirements for utilizing renewable energy to substitute traditional energy.[1–4] Among the strategies of effectively storing energy, electrochemical capacitors, also named supercapacitors, are a kind of promising devices for energy storage due to their long cycle life, superior power density and good rate ability.[3–6] Besides concentration on improving the electrochemical performance of supercapacitors,[7–13] integration with multi-functions, such as flexibility and wearable compatibility,[14–23] has increasingly attracted the interests of researchers for convenient usage of supercapacitors in portable devices. In addition, incorporating some smart functionalities to supercapacitors for easy uses in daily lives is another important issue for developing supercapacitors.[24–26] Among these issues, it is important to allow people to easily and real-timely estimate or determine the storage of electrical energy. Therefore, using or incorporating smart materials that can be used for easily determining the electrical energy storage is of great significance.[27–32]

For easy estimation of energy storing states, variation of the active materials should be easily sensed by human. The visual change is the most impressive change to be identified. Meanwhile, some transition-metal oxides or conductive polymers (e.g. polyaniline) can serve as active materials for both supercapacitors and electrochromic devices because they all utilize the fast faradic reactions between the active materials and electrolytes.[33–36] Therefore, these kind of materials are suitable for fabrication of smart supercapacitors. Among these materials, tungsten oxides have been reported being used as smart materials for supercapacitors due to their great compatibility for both supercapacitors and electrochromic devices, as well as the perfect contrast between bleached state (transparent) and colored state (dark blue). The smart function has been successfully demonstrated by relating the change of color to potential or electrical energy storage (EES) of the working electrode.[27–33]

In spite of these demonstrations, at least three problems should be resolved to achieve an impeccable smart function. First of all, the color change can only be used for estimation, while how to quantitatively define color change and thus determine the associated supercapacitors' parameters remain challenges. Secondly, only very few materials that are active for both electrochromic and electrochemical capacitor can be

[a] *Department of Physics and Materials Science, City University of Hong Kong, 83 Tat Chee Avenue, Kowloon, Hong Kong*
[b] *School of Mechanical, Electrical & Information Engineering, Shandong University, Weihai, P.R. China*
[c] *Shenzhen Research Institute, City University of Hong Kong, Shen Zhen, 518057, P.R. China*

† Electronic Supplementary Information (ESI) available: XRD patterns of e-$WO_3$, table of the electrical energy storage (EES) obtained from the idea and tested galvanostatic curves, transmission spectrum when EES is 0%, cyclic voltammetric and galvanostatic curves of e-$WO_3$//PPy and e-$WO_3$//$MnO_2$. See DOI: 10.1039/x0xx00000x

used as electrodes of this kind of smart devices. As a result, the reported color-change smart supercapacitors usually possess limited capacitance;[29,31] while the smart function has not been realized for the high performance supercapacitors fabricated by excellent active materials, such as PPy and $MnO_2$.[37–40] Therefore, it is of great importance to develop a practicable approach to integrate the smart functions and highly capacitive performance.

The third problem is a crucial and essential one: it is actually not clear that the color change should be associated with potential or EES of the supercapacitors. It should be noted that, the dependence between potential and EES is not linear. This is because the galvanostatic curves tested for almost all types of supercapacitor electrodes, especially the pseudo ones always present a serious distortion from an ideal triangle, as displayed in Fig. 1a, a typical galvanostatic curve for a $WO_3$ electrode. Therefore, a great deviation may be generated if calculating EES from potential by the popularly used equation EES= $(E_{EES}–E_0)/\Delta E$, where $E_{EES}$ is the potential at the certain EES, $E_0$ is the potential at initial state, and $\Delta E$ is the potential window. As shown in Fig. 1b, the intersection points of the grid intersection represent the calculated EES based on the assumption that the potential is linearly related to the time, which are emphasized by the magenta dots. The blue circle and red diamond dots represent the actual EES calculated from the real charging and discharging curves, respectively. It is revealed that the deviation can reach as large as 16.27% (Table S1 in the supporting information). Therefore, it becomes very important to clearly figure out the color change is actually associated with potential or EES of a supercapacitor, or clarify how to associate color change to EES that is usually considered as an essential parameter for a supercapacitor as an energy storage device.

To solve three problems mentioned above, herein, tungsten oxide ($WO_3$) was synthesized by a very facile electrodepositing method as the smart electrode materials. Optical density, a concept in electrochromism study is introduced for a comprehensive investigation on the color change of the $WO_3$ film based supercapacitors. Then, a linear dependence between normalized optical density and EES of the supercapacitor is discovered, which enables a precisely quantitative determination of the EES of the supercapacitor.

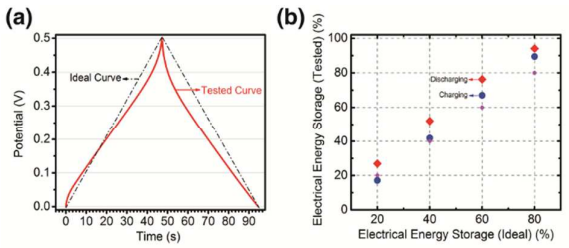


Fig. 1 Using potentials to estimate EESs of a supercapacitor through a simple equation may result in serious deviation due to nonlinear dependence between them. (a) The deviation of ideal triangular galvanostatic curve from the tested one of an e-$WO_3$ electrode, and (b) the deviation of the EESs calculated from the ideal curve from those calculated by the tested curve. The charged and discharged EESs are represented by the red diamond dots and blue circle dots, respectively. The ideal EESs are indicated by the intersections of the grids, and they are highlighted by the magenta circle dots.

Subsequently, hybrid supercapacitors were successfully designed and fabricated in order to integrate the smart function of color-change based EES indicator to various high-performance supercapacitors. The calibration curves were developed for different hybrid supercapacitors, which makes it easy to quantitatively determine EES of high-performance supercapacitors precisely by a simple optical transmission test.

## 2. Experimental

### 2.1. Fabrication of the e-$WO_3$ based solid-state supercapacitors

$WO_3$ was electrodeposited to the surface of a FTO coated glass. The aqueous solution for the electrodeposition was prepared by the process as follow: $Na_2WO_4$ (1.65g) was dissolved in deionized water (200mL) followed by adding $H_2O_2$ (0.6mL) under stirring. Subsequently, the pH of the electrolyte was adjusted to be 1.5 by adding $HNO_3$ (3M). Afterwards, the electrodeposition process was carried out under the constant voltage (-0.65 V vs. SCE) and lasted 300s for a balance between the transparency of the electrode and the capacitance. The weight is around 1mg. The electrolyte for solid-state supercapacitors was prepared by the following process: $H_2SO_4$ (6g) was mixed with deionized water (60mL) followed by adding PVA (6g, molecular weight: ~100000). Subsequently, the mixture was heated to 85°C under stirring. When the mixture became transparent, the prepared electrodes were immersed into the hot electrolyte and kept for several seconds. After the electrolyte solidified, two electrodes was intersected assembled.

### 2.2. Fabrication of the hybrid solid-state supercapacitors

For the e-$WO_3$//PPy hybrid electrodes, the e-$WO_3$ was electrodeposited onto one zone of the FTO coated glass. Then, the PPy was electrochemical polymerized under constant voltage of 0.8V onto the other zone of the FTO coated glass using the aqueous solution containing p-Toluenesulfonic acid (0.1M), sodium p-Toluenesulfonic (0.3M), and pyrrole monomer (300μL) for 90s. The weight of PPy formed on the FTO is around 0.5mg. The assembling process is similar to that of e-$WO_3$ based solid-state supercapacitor. For fabrication of e-$WO_3$//$MnO_2$ hybrid supercapacitors, the $MnO_2$ was electrodeposited using the electrolyte containing $Mn(NO_3)_2$ (20mM) and $NaNO_3$ (100mM) under the constant current density of 0.5 mA $cm^{-2}$. The weight of MnO2 formed on the FTO is around 0.5mg. The assembling process was identical to that of e-$WO_3$//PPy hybrid solid-state supercapacitors.

### 2.3. Electrochemical Tests and Materials Characterizations

Electrochemical measurements were carried out on an electrochemical workstation (CHI660C). The crystallographic characters of samples were investigated with a X-ray Powder

Diffraction using BRUKER D2 PHASER diffractometer, which was equipped with Cu Kα irradiation (λ = 1.54184 Å) and working at 10 mA and 30 kV. The morphologies were investigated by environmental scanning electron microscope (ESEM, FEI/Philips

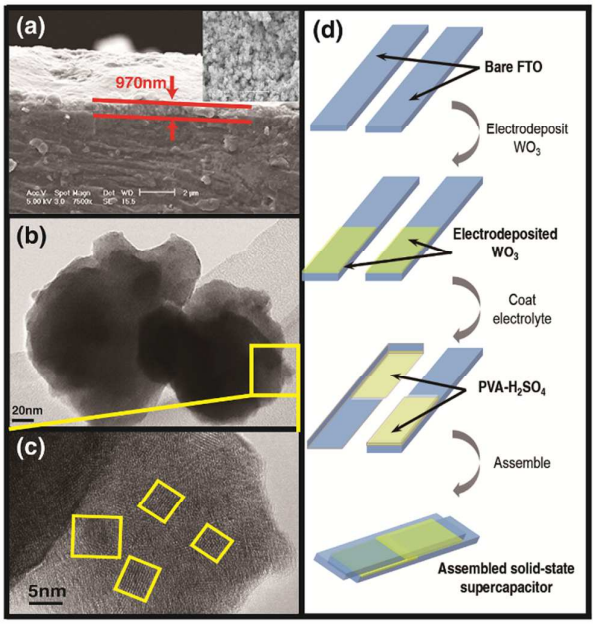


Fig. 2. (a) Cross-section SEM image of the e-$WO_3$ film, (b) TEM and (c) HRTEM images of the e-$WO_3$ nanoparticles. (d) Schematic of the process for fabrication of the e-$WO_3$ solid-state supercapacitors.

XL30), field emission transmission electron microscope (JEOL-2001F). UV-vis experiments were made under transmission mode with a UV-Vis spectrophotometer (HALO DB20) over a wavelength range of 400-800 nm.

## 3. Results and discussion

### 3.1. Electrochromic Supercapacitor and its EESs

Fig. 2a shows the scanning electron microscopy (SEM) images of the cross-section of the electrode based on e-$WO_3$. The thickness of the e-$WO_3$ film is about 970 nm, which not only enables sufficient coloring efficiency but also maintains the transparency of the electrode on bleached state. It consists of the nanoclusters of e-$WO_3$ nanoparticles, which is shown in the inset in Fig. 2a. The transmission electron microscopy (TEM) image in Fig. 2b confirms the particle structures of the e-$WO_3$ film. Fig. 2c shows the high resolution trasmission electron microscopy (HRTEM) image of e-$WO_3$, which reveals a structure by embedding many small crystal nanoparticles in an amorphous matrix. This structure observed is in consistent with the XRD patterns shown in Fig. S1 in the supporting information, which shows a broad peak combined with several sharp peaks, corresponding to the amorphous and crystallized components of the e-$WO_3$ nanoparticle clusters. The crystal structure identified from the XRD patterns shows that the e-$WO_3$ is cubic phase (JCPDS no. 41-0905, cubic, Pm/3m). The amorphous matrix will benefit the electrochromic process due to its good stability and high contrast between bleached and colored state.[42,43] Scheme in Fig. 2d shows the process of fabricating electrodeposited tungsten oxide (e-$WO_3$) based solid state supercapacitors. Briefly, e-$WO_3$ was electrodeposited onto the two FTO coated glasses, followed by coating the electrolyte (PVA-$H_2SO_4$). After the solidification of the electrolyte, as-prepared two FTO coated glasses was assembled together intersected for easy observation of the color variation at different EESs.

To reveal the electrochemical properties, the e-$WO_3$ film was firstly investigated in liquid electrolyte (0.5M $H_2SO_4$) between the potential ranging from -0.5V ~ 0V referred to the saturated calomel electrode (SCE). Fig. 3a,b shows the cyclic voltammetric (CV) and galvanostatic curves. In addition to the near rectangular and symmetric shape of CV curves measured at low scan rates of 5 ~ 20 mV $s^{-1}$, anodic and cathodic peaks of e-$WO_3$ can also be clearly identified. These are typical features for pseudocapacitors, indicating redox reactions are involved while great reversibility kept. The obvious distortion of CV curves can be found under high scan rates (> 50 mV $s^{-1}$), which results from the limited conductivity and time constant of the e-$WO_3$ film.[34] The galvanostatic curves (Fig. 3b) shows the distortion from the ideal triangle with near symmetric shapes, which also represents a pseudocapacitive process. The area capacitance, which is believed more reliable and practical, especially when the weight of active materials is very small, is accordingly used here.[41] And the area capacitance calculated from the galvanostatic curve reaches 10 mF $cm^{-2}$ at the charging and discharging current of 0.05 mA $cm^{-2}$, showing the decent capability of e-$WO_3$ as active materials of supercapacitors. Fig. 3c, d show typical CV and galvanostatic curves for the all solid-state supercapacitors with e-$WO_3$ electrodes. Typical pseudocapacitive behaviors are kept and the area capacitance e-$WO_3$ based solid-state supercapacitors reaches 3.5 mF $cm^{-2}$ for the device and 7.0 mF $cm^{-2}$ for the single electrode at the charging and discharging current of 0.05 mA $cm^{-2}$. This performance is comparable with other electrochromic supercapacitors based on $WO_3$ as can been seen in Table S2. The decrease of the capacitance in solid-state device is the result of the increase of the bulk resistance and more sluggish capacitive behavior due to the relatively poor contact between the e-$WO_3$ and solid-state electrolyte, which can be seen from Nyquist plots in Fig. S2.

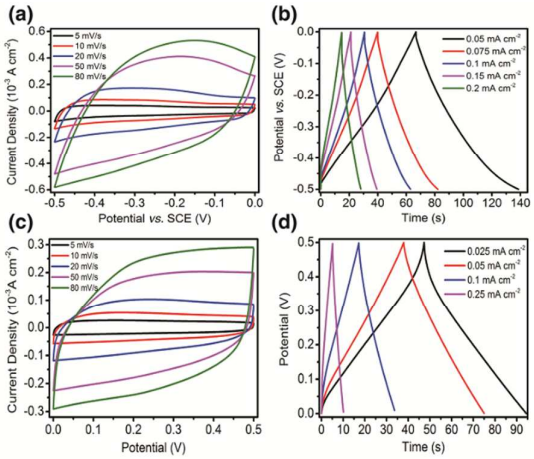


Fig. 3. (a) CV and (b) galvanostatic curves of the e-$WO_3$ in 0.5 M $H_2SO_4$ electrolyte, (c) CV and (d) galvanostatic curves of the e-$WO_3$ in the solid-state supercapacitors.

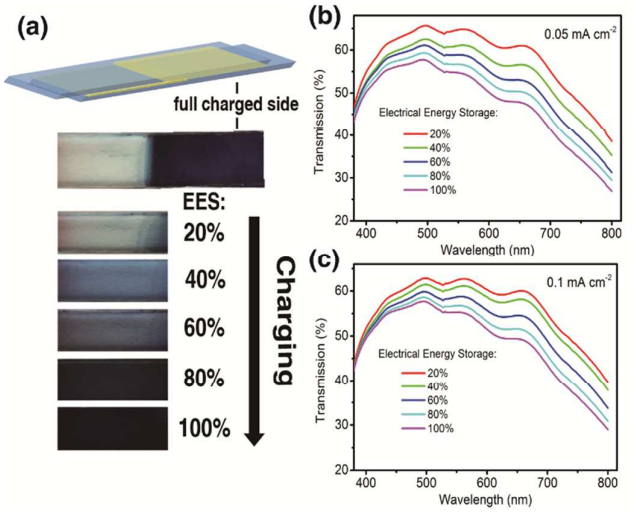


Fig. 4 (a) Photographs of the e-$WO_3$ electrode at different EESs, and the transmission spectra of the e-$WO_3$ electrode charged at different currents: (b) 0.1mA, (c) 0.2mA.

For further confirmation of the capability of e-$WO_3$ serving as active materials for electrochromic supercapacitors, we took the SEM images of e-$WO_3$ after electrochromic and electrochemical process (Fig. S3). As no significant difference can be seen from Fig. S3, the as-prepared e-$WO_3$ is suitable for being active materials for electrochromic supercapacitors.

Accompany with the energy storage by the reaction: $WO_3 + xH^+ + xe^- \rightarrow H_xWO_3$, the electrode will change from transparent to dark blue due to the increasing formation of blue colored center $W^{+5}$ polarons.[44-46] Photos in Fig. 4a show the color of the electrodes at different EES, which certificates the color change as expected. The electrode at pristine state (EES = 0%) is almost transparent. During charging process, the color becomes darker and darker with the EES increasing from 0% to 100%. A fully charged (EES = 100%) supercapacitor exhibits a dark blue appearance with the $W^{+5}$ heavily formed. Therefore, the EES can be easily estimated by identifying the color of the electrodes.

The next target is to quantitatively determine EES of the supercapacitor by color change. Transmission spectra of the electrode were measured at the wavelength range of 400 to 800 nm under charging/discharging current of 0.05 mA $cm^{-2}$ and 0.1 mA $cm^{-2}$, respectively. It was revealed that the transmission continuously decreases during the charging process for both charging current densities. However, detailed comparison indicates that the variation at red light region (620-750 nm) is much more remarkable than that at blue light region (450-475 nm). For example, with the supercapacitor being charged at 0.05 mA $cm^{-2}$ to 100% EES (Fig. 4b), the transmission at wavelength of 625 nm decreases around 29%, while it is 9% for the wavelength of 450 nm. Greater loss of the red light transmission finally results in dark blue color of the electrodes at high EES, which is in accordance with the photos shown in Fig. 4a. Therefore, the transmission at the red light region (for example, the wavelength of 625 nm) can be an excellent indicator for the EES of the e-$WO_3$ based solid-state-supercapacitor.

Here we introduce a concept popularly used in electrochromic studies, optical density, for further quantitative analyses.[30,32,33,42-47] The optical density is defined as log ($T_{bleached}/T_{colored}$), where $T_{bleached}$ is the transmission in the bleached state, and $T_{colored}$ is related to the different transmission during the electrochromic process. Furthermore, it is well known that the relationship between the optical density and the charge consumed during the electrochromic process ($Q_c$) can be expressed as:

$$\log (T_{bleached}/T_{colored}) = \eta \times Q_c \quad (1)$$

Here, η means the coloring efficiency of the as-prepared material, which is a constant because it is related to the nature of the as-prepared material.[30,32,33,42-47] Since the electrochromic process also means the charging process for the electrochromic supercapacitors, we can regard the $T_{bleached}$ as the transmission at 0% EES ($T_0$), and $T_{colored}$ as the transmission at different EESs ($T_{EES}$). Moreover, $Q_c$ can be expressed as $Q_c$=EES×$Q_t$, where $Q_t$ is the total charge can be stored in the electrochromic supercapacitors at certain situation. Therefore, the color change at different EES can be quantifiably expressed by the equation:

$$\log (T_0/T_{EES}) = \eta \times EES \times Q_t \quad (2)$$

Since the value of $Q_t$ may be different at different charging and discharging rate, the optical density is normalized by the $Q_t$ at certain charging and discharging rate. And the normalized optical densities of 625 nm versus corresponding EESs are plotted in Fig. 5a, b. Accordingly, a linear dependence is clearly revealed. The fitted curve by y = Ax+B is plotted as dashed lines in Fig. 5a,b. The fitted correlations (R) at different charging/discharging currents are both very close to 1 (0.99 for both 0.05 mA $cm^{-2}$ and 0.1 mA $cm^{-2}$), which indicates a perfect linear dependence in spite of the charging/discharging currents. By using these fitted curves, we can use the normalized optical density to reveal the EES of the

supercapacitors. Furthermore, the difference between values calculated from these two curves is less than 2% as shown in Table S3 in SI, which indicates the perfect accuracy. The introduction of optical density and its linear dependence with EES open a way to quantitatively and precisely determine the EESs of a supercapacitor with a simple optical transmission measurement by a spectrophotometer.

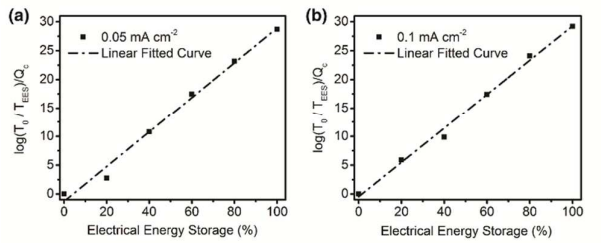


Fig. 5 Optical densities at 625 nm versus EESs at charging/discharging current of 0.1 mA (a) and 0.2 mA (b), respectively. A linear dependence is clearly revealed.

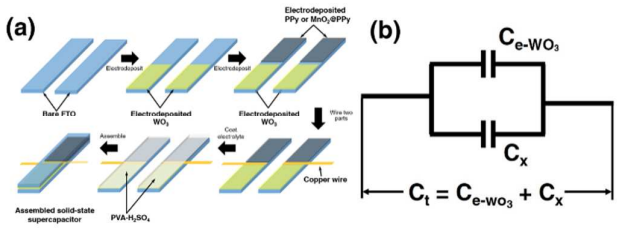


Fig. 6 (a) Schematic illustration of the fabrication process of the e-$WO_3$ based hybrid solid-state supercapacitors, and (b) Equivalent circuit the fabricated hybrid supercapacitors.

Back to the three problems mentioned in the introduction part, here we clarify that the color change is more related to the EES of a supercapacitor instead of the potential. In addition, the optical density can be used to quantify the color change of the electrodes and it linearly dependents on the EESs of a supercapacitor with $WO_3$ as electrodes, which can serve as the indicator of EES for electrochromic supercapacitors.

### 3.2. Hybrid Supercapacitors with Electrochromic EES Indicator

To extend the applications of the developed smart supercapacitor and to solve the problem of limited capacitance of the e-$WO_3$ electrodes, we developed and investigated the hybrid solid-state supercapacitors that integrate smart function of e-$WO_3$ to various high-performance supercapacitors. For the universality, we choose two most popular supercapacitor materials, PPy and $MnO_2$ as electrochemically active materials to investigate the relationship between the coloring process of the e-$WO_3$ part and the charging process of the whole device. The fabricating process is schematically shown in Fig. 6a. Briefly, $WO_3$ was deposited on the one zone of FTO coated glass, followed by PPy or $MnO_2$ being electrodeposited on the other zone. A cooper wire is bridged between two zones to form a parallel connection structure (Fig. 6b). Afterwards, coating electrolyte and assembling two pieces of electrodes were done to form a hybrid solid-state supercapacitor. It is expected that with the parallel structure (Fig. 6b), the hybrid solid-state supercapacitors may take advantages of both smart function of e-$WO_3$ and high capacitance from the highly capacitive active materials.

The electrochemical performance of as-prepared hybrid supercapacitors was investigated by the CV and galvanostatic tests. Fig. 7a and Fig. S4 show the CV curves of hybrid supercapacitors of the e-$WO_3$ incorporated with the electrodeposited PPy (e-$WO_3$//PPy) and $MnO_2$ (e-$WO_3$//$MnO_2$). All curves measured at 20 mV $s^{-1}$ in Fig. 7a exhibit typical pseudocapacitive behaviors. The distortion of the CV curve of e-$WO_3$//$MnO_2$ is severer than others due to the involved redox reactions and relatively low conductivity of the $MnO_2$. The greatly improved capacitive performance after incorporating the PPy or $MnO_2$ are clearly indicated by the dramatically enlarged CV encircled area. The capacitances of the e-$WO_3$//PPy and the e-$WO_3$//$MnO_2$ at the high scan rate (20 mV $s^{-1}$) can reach 11.38 and 14.21 mF $cm^{-2}$, respectively, which are ~ 5 times and 7 times higher than that of pure e-$WO_3$ based supercapacitors (2.22 mF $cm^{-2}$) at the same scan rates. The enhancement of capacitance can be intuitionally confirmed by

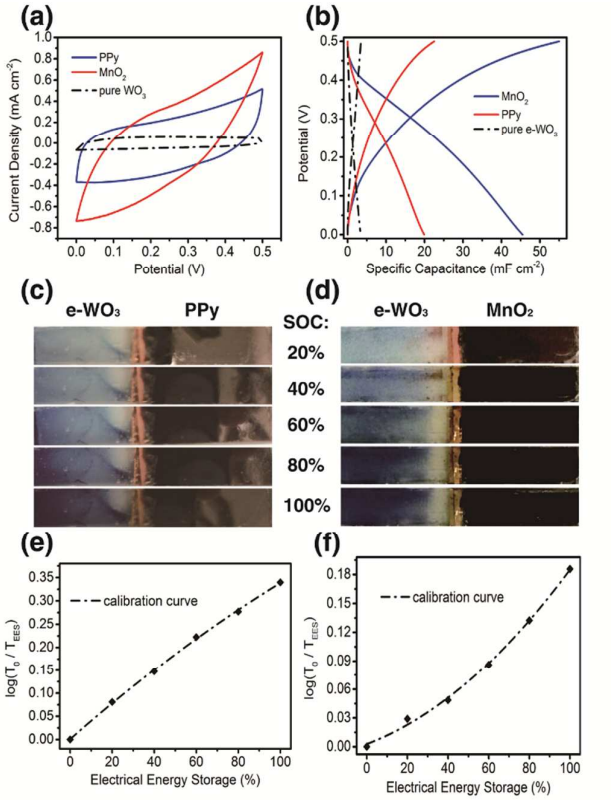


Fig. 7 (a) CV curves of the e-$WO_3$//PPy and e-$WO_3$//$MnO_2$ based hybrid supercapacitors at 20 mV $s^{-1}$; (b) galvanostatic charging/discharging curves of the e-$WO_3$//PPy and e-$WO_3$//$MnO_2$ based hybrid supercapacitors measured at a current density of 1 mA $cm^{-2}$; photos of the electrodes of the e-$WO_3$//PPy hybrid supercapacitors at different EESs (c) and e-$WO_3$//$MnO_2$ hybrid supercapacitors at different EESs (d); optical densities at 625 nm versus EESs of the e-$WO_3$//PPy hybrid supercapacitors (e) and the e-$WO_3$//$MnO_2$ hybrid supercapacitors (f), which can be considered as a unique calibration curve solely produced for each type of hybrid supercapacitors.

the galvanostatic curves shown in Fig. 7b. (Fig. S4 as well). At the charging/discharging rate of 1 mA $cm^{-2}$, the capacitance enhancement is more obvious.

As shown in Fig. 7b, the e-$WO_3$//$MnO_2$ hybrid supercapacitor possesses a capacitance of 45 mF $cm^{-2}$, which is much higher than that of pure e-$WO_3$ based supercapacitor. Also, these impressive capacitance achieved by hybrid supercapacitors is much larger than other electrochromic supercapacitors without the hybrid design, as shown in Table S2.

Besides the greatly enhanced performances, the smart function is also well maintained. The photos of electrodes of the hybrid supercapacitors at different EESs are shown in Fig. 7c, d. Evidently, the color changes for the hybrid supercapacitors are visibly identical to that of the pure e-$WO_3$ based supercapacitors shown in Fig. 4a. In addition, the EES of the capacitor can be accurately and quantifiably indicated by the normalized optical density due to the fixed relationship between them for as-prepared e-$WO_3$ as described by Equation 2. Based on this, the EESs of the hybrid supercapacitors may also be quantitatively determined by a simple optical transmission measurements, followed by calculating optical density at 625 nm.

However, it should be noted that EES obtained here represents the EES of the whole device. And this EES may not be identical to the EES of the e-$WO_3$ part ($EES_w$) due to the hybrid charging/discharging dynamic. But, there will be a relationship between EES and $EES_w$ ($EES_w$=*f*(EES)). Thus, the relationship between the optical density and the EES can be revised as:

$$\log (T_0/T_{EES})=\eta\times f(EES)\times Q_w \quad (3)$$

where η, the coloring efficiency, is just related to the nature of the as-prepared e-$WO_3$, and $Q_w$ will be a constant at the certain charging and discharging rate. Herein, the dependence between optical densities at 625 nm and EESs of hybrid supercapacitors might be revealed by a calibration curve. Fig. 7e, f exhibit the optical densities at 625 nm *vs.* the representative EESs (0%, 20%, 40%, 60%, 80% and 100%) for the electrodes of e-$WO_3$//PPy and e-$WO_3$//$MnO_2$, respectively. The e-$WO_3$//PPy hybrid supercapacitor exhibits a convex calibration curve while the e-$WO_3$//$MnO_2$ hybrid supercapacitor shows a concave calibration curve, as shown in Fig. 7e and f, respectively. The shape of the calibration curves include information of the hybrid charging/discharging processes. As long as the calibration curves are generated, the EESs of any types of hybrid supercapacitor can be quantitatively determined by a simple optical transmission measurement. For example, an optical density of 0.11 and 0.31 at 625 nm represent an EES of 30% and 90%, respectively, for the e-$WO_3$//PPy hybrid supercapacitors. Based on the analysis before, the EES of the hybrid supercapacitors can be visually indicated by the color change of the e-$WO_3$ and quantifiably determined by the calibration curves, which means e-$WO_3$ can be integrated with other active materials to form a smart hybrid supercapacitors.

## Conclusions

In conclusion, three progresses on smart supercapacitors were achieved in this paper. 1. A visualized indicator was developed for supercapacitor devices by using the e-$WO_3$ as active material. The color change of the electrode can be used to estimate potential and EES of the supercapacitor. 2. By introducing concepts in electrochromic studies and detailed investigations of optical spectra of the supercapacitor, the normalized optical densities were found to linearly depend on the EESs of the e-$WO_3$ based supercapacitor. This finding quantifies the color change of the e-$WO_3$ electrodes, as well as clarifies that, instead of potential, EESs can be associated with color change directly. In addition, this finding makes it possible to quantitatively determine the EESs of the supercapacitor by a simple optical transmission test. 3. Hybrid supercapacitors with parallel structure were developed in order to integrate color-change EES indicator for high performance supercapacitors. Utilizing the method developed, the e-$WO_3$ electrode based EES indicator can be integrated into any types of supercapacitors to achieve both high capacitive performances and the smart functions. In addition, we establish a strategy to produce a calibration curve for each type of hybrid supercapacitors, which enable quantitatively determine their EESs precisely by a simple optical transmission measurement. The approaches developed in this research make it possible to equip color-change based EES indicator for any energy storage device and determine their EES easily by a simple optical transmission measurement. Moreover, due to the principal of this EES indicator is based on the electrochromic phenomenon of e-$WO_3$, which can be continuously colored with charging process, it can also be used as the EES indicator for asymmetric supercapacitors, whose potential window is larger. Thus, the application areas can be wider. These may greatly extend applications of the electrochromic materials in energy storage devices for smart function integrations.

## Acknowledgements

This research was partial supported by a grant from the Research Grants Council of the Hong Kong Special Administrative Region, China (Project No. CityU 109213), the Science Technology and Innovation Committee of Shenzhen Municipality (the Grant No. JCYJ20140419115507579).

## Notes and references

1 J. Miller, P. Simon, Science, 2008, **321**, 651-652.
2 P. Simon, Y. Gogotsi, Nat. Mater., 2008, **7**, 845-854.
3 H. Guan, X. Wang, H. Li, C. Zhi, T. Zhai, Y. Bando, D. Golberg, Chem. Commun., 2012, **48**, 4878-4880.
4 X. Wang, W. Tian, D. Liu, C. Zhi, Y. Bando, D. Golberg, Nano Energy, 2013, **2**, 257-267.
5 N. Kumar, H. Choi, Y. Shin, D. Chang, L. Dai, J. Baek, ACS Nano, 2012, **6**, 1715-1723.
6 T. Chen, L. Dai, Mater. Today, 2013, **16**, 272-280.

7 W. Meng, W. Chen, L. Zhao, Y. Huang, M. Zhu, Y. Huang, Y. Fu, F. Geng, J. Yu, X. Chen, C. Zhi, Nano Energy, 2014, **8**, 133-140.
8 Q. Weng, X. Wang, X. Wang, C. Zhang, X. Jiang, Y. Bando, D. Golberg, J. Mater. Chem. A, 2015, **3**, 3097-3012.
9 D. Liu, X. Wang, X. Wang, W. Tian, J. Liu, C. Zhi, D. He, Y. Bando, D. Golberg, J. Mater. Chem. A, 2013, **1**, 1952-1955.
10 X. Wang, Y. Zhang, C. Zhi, X. Wang, D. Tang, Y. Xu, Q. Weng, X. Jiang, M. Mitome, D. Golberg, Y. Bando, Nat. Comm., 2013, **4**, 2905.
11 Y. Qian, R. Liu, Q. Wang, J. Xu, D. Chen, G. Shen, J. Mater. Chem. A, 2014, **2**, 10917-10922.
12 W. Tian, X. Wang, C. Zhi, T. Zhai, D. Liu, C. Zhang, D. Golberg, Y. Bando, Nano Energy, 2013, **2**, 754-763.
13 Z. Ma, X. Huang, S. Dou, J. Wu, S. Wang, J. Phys. Chem. C, 2014, **118**, 17231-17239.
14 X. Lu, T. Zhai, X. Zhang, Y. Shen, L. Yuan, B. Hu, L. Gong, J. Chen, Y. Gao, J. Zhou, Y. Tong, Z. Wang, Adv. Mater., 2012, **24**, 938-944.
15 L. Gao, X. Wang, Z. Xie, W. Song, L. Wang, X. Wu, F. Qu, D. Chen, G. Shen, J. Mater. Chem. A, 2013, **1**, 7167-7173.
16 N. Liu, W. Ma, J. Tao, X. Zhang, J. Su, L. Li, C. Yang, Y. Gao, D. Golberg, Y. Bando, Adv. Mater., 2013, **25**, 4925-4931.
17 T. Chen, Y. Xue, A. Roy, L. Dai, ACS Nano, 2013, **8**, 1039-1046.
18 J. Bae, M. Song, Y. Park, J. Kim, M. Liu, Z. Wang, Angew. Chen. Int. Ed., 2011, **50**, 1683-1687.
19 L. Yuan, X. Lu, X. Xiao, T. Zhai, J. Dai, F. Zhang, B. Hu, X. Wang, L. Gong, J. Chen, C. Hu, Y. Tong, J. Zhou, Z. Wang, ACS Nano, 2012, **6**, 656-661.
20 D. Y, K. Goh, H. Wang, L. Wei, W. Jiang, Q. Zhang, L. Dai, Y. Chen, Nat. Nanotechnol., 2014, **9**, 555-562.
21 L. Yuan, B. Yao, B. Hu, K. Huo, W. Chen, J. Zhou, Energy Environ. Sci., 2013, **6**, 470-476.
22 Y. Huang, M. Zhu, W. Meng, Y. Fu, Z. Wang, Y. Huang, Z. Pei, C. Zhi, RSC Adv., 2015, **43**, 33981-33989.
23 S. Wang, B. Pei, X. Zhao, R. Dryfe, Nano Energy, 2013, **2**, 530-536.
24 J. Xu, H. Wu, L. Lu, S. Leung, D. Chen, X. Chen, Z. Fan, G. Shen, D. Li, Adv. Funct. Mater., 2014, **24**, 1840-1846.
25 X. Wang, B. Liu, R. Liu, Q. Wang, X. Hou, D. Chen, R. Wang, G. Shen, Angew. Chen. Int. Ed., 2014, **53**, 1849-1853.
26 P. Yang, X. Xiao, Y. Li, Y. Ding, P. Qiang, X. Tan, W. Mai, Z. Lin, W. Wu, T. Li, H. Jin, P. Liu, J. Zhou, C. Wong, Z. Wang, ACS Nano, 2013, **7**, 2617-2626.
27 X. Chen, H. Lin, J. Deng, Y. Zhang, X. Sun, P. Chen, X. Fang, Z. Zhang, G. Guan, H. Peng, Adv. Mater., 2014, **26**, 8126-8132.
28 P. Yang, P. Sun, Z. Chai, L. Huang, X. Cai, S. Tan, J. Song, W. Mai, Angew. Chem. Int. Ed., 2014, **126**, 12129-12133.
29 Y. Tian, S. Cong, W. Su, H. Chen, Q. Li, F. Geng, Z. Zhao, Nano Lett., 2014, **14**, 2150-2156.
30 B. Reddy, P. Kumar, M. Deepa, ChemPhysChem, 2015, **16**, 377-389.
31 Z. Xie, X. Jin, G. Chen, J. Xu, D. Chen, G. Shen, Chem. Commun., 2013, **50**, 608-610.
32 H. Wei, X. Yan, S. Wu, Z. Luo, S. Wei, Z. Guo, J. Phys. Chem. C, 2012, **116**, 25052-25064.
33 G. Cai, X. Wang, M. Cui, P. Darmawan, J. Wang, A. Eh, P. Lee, Nano Energy, 2015, **12**, 258-267.
34 M. Zhu, W. Meng, Y. Huang, Y. Huang, C. Zhi, ACS Appl. Mater. Interfaces, 2014, **6**, 18901-18910.
35 D DeLongchamp, PT Hammond, Adv. Mater., 2001, **13**, 1455-1459.
36 BP Jelle, G Hagen, Sol. Energ. Mat. Sol. C., 1999, **58**, 277-286.
37 J. Tao, N. Liu, W. Ma, L. Ding, L. Li, J. Su, Y. Gao, Sci. Rep., 2013, **3**, 2286.
38 J. Tao, N. Liu, L. Li, J. Su, Y. Gao, Nanoscale, 2014, **6**, 2922-2928.
39 Y. Huang, J. Tao, W. Meng, M. Zhu, Y. Huang, Y. Fu, Y. Gao, C. Zhi, Nano Energy, 2015, **11**, 518-525.
40 Y. Huang, Y. Huang, W. Meng, M. Zhu, H. Xue, C. Lee, C. Zhi, ACS Appl. Mater. Interfaces, 2015, **7**, 2569-2574.
41 Y. Gogotsi, P. Simon, Science, 2011, **334**, 917-918.
42 J. Wang, E. Khoo, P.S. Lee, J. Ma, J. Phys. Chem. C, 2008, **112**, 14306-14312.
43 O. Schirmer, V. Wittwer, G. Baur, G. Brandt, J. Electrochem. Soc., 1977, **5**, 749-753.
44 E. Ozkan, S. Lee, C. Tracy, J. Pitts, S. Deb, Sol. Energ. Mat. Sol. C., 2003, **4**, 439-448.
45 J. Zhang, D. Benson, C. Tracy, S. Deb, A. Czanderna, C. Bechinger, J. Electrochem. Soc., 1997, **6**, 2022-2026.
46 C. Li, J. H. Hsieh, M. Hung, B.Q. Huang, Thin Solid Films, 2015, **587**, 75-82.
47 S. Lee, R. Deshpande, P. Parilla, K. Jones, B. To, A. Mahan, A. Dillon, Adv. Mater., 2006, **6**, 763-766.

Table of contents:

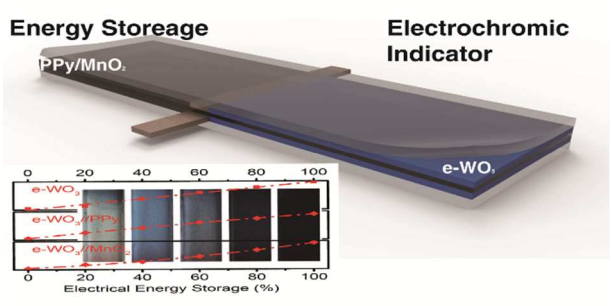


Quantifiably determining electrical energy storage of solid-state supercapacitors is fulfilled by integrating electrochromic tungsten oxide electrodes.